2023 IEEE International Conference on Robotics and Automation (ICRA 2023)
May 29 - June 2, 2023. London, UK

Soft Sensing Skins for Arbitrary Objects: An Automatic Framework

Sonja Groß*,1,2, Diego Hidalgo-Carvajal*,1,2, Silija Breimann[1], Nicolai Stein[1], Amartya Ganguly[1], Abdeldjallil Naceri[1], and Sami Haddadin[1,2]

***Abstract*— Tactile sensors are becoming more prevalent in numerous research domains, including robotics, human-robot interaction, and grasping. As the development of customized soft tactile skin for various applications continues to gain momentum, there is an increasing demand for the automation of design and manufacturing processes based on user specifications. Our work presents a partially automated framework for designing and customizing silicone-based skin-like sensors for objects of arbitrary shapes. We assess the performance of stretch and contact sensors featuring custom patterns on complex surfaces, subjecting them to position control, grasping, and manipulation scenarios. Our study's findings demonstrate the feasibility of fabricating skin-like sensors effectively within a semi-automated framework, with potential applications in the aforementioned research domains.**

I. INTRODUCTION

Tactile sensing technologies have the potential to endow robotic systems with the ability to perceive their surroundings with a similar level of complexity as that of their human counterpart. Furthermore, they can elucidate insights into manipulation and human-object interactions. The multidisciplinary nature of sensorization technologies can help expedite the number of applications for robotics, and is, therefore, a crucial topic to undertake. Although there have been several developments in soft tactile sensors [1], [2], only a few studies have looked into ways to accelerate and customize their development and applications. In this study, we combine four areas to close this gap, namely, UV-unwrapping, automated manufacturing of silicone-based contact and strain sensors, strain-sensor-based finger motion control and object contact detection.

Table I summarizes developments in pressure and strain sensitive soft tactile skin with myriad applications from sensorized objects for grasp analysis to robotics and wearables. In recent years, 3D printing technology has simplified the manufacturing of such sensors [3]–[5]. In particular, embedded 3D (e-3D) printing overcomes prior limitations such as extensive multistep polymer casting and poor shape fidelity by enabling the deposition of conductive ink into an extensible elastomer matrix [6], [7]. This has led to strain sensors with a predictable resistance change up to 400% [8]. Additionally, studies such as the ones proposed by [5], [9], [10] have presented the research community with interfaces in which tactile sensors can be semi-automatically designed and manufactured. Research in the field of UV unwrapping, as proposed by the authors of [11]–[14] has shown satisfactory results when creating 2D surface representations of 3D models. Nevertheless, they have been under utilized for the automated design and manufacturing of silicon-based, stretchable tactile skins. In this work we have applied capabilities of these algorithms, particularly the one proposed in [11], to map arbitrary 3D objects into 2D surfaces, serving as an input to the e-3D printing platform presented in [15] to automatically generate sensing skins for arbitrary objects, including models of human and robot fingers.

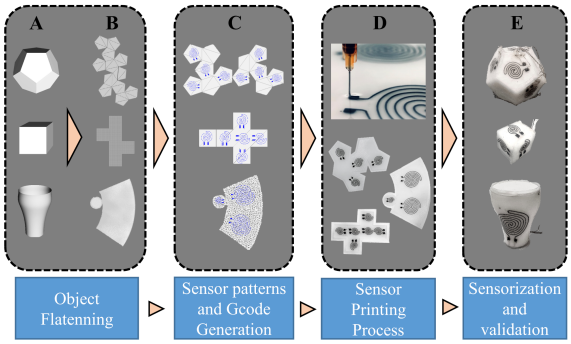

Fig. 1. Overview of our proposed framework. A shows rigid input objects to our framework, B shows the objects' flattened surfaces, C shows the sensing pattern placement using our tool, D shows the sensor printing process, and E shows resulting sensors and their placement on the objects.

TABLE I

OVERVIEW OF SOFT SENSITIVE SKINS. ABBREVIATIONS: DESIGN (D), MANUFACTURING (M), ASSEMBLY (A), MANUAL (X), PARTIALLY AUTOMATED (O), FULLY AUTOMATED (√).

Publication	Application	Modalities	Manufacturing	Conformability	Automation		
					D	M	A
Koiva et al. [16]	grasp analysis	pressure	polymer casting	rigid	x	x	x
Bücher et al. [17]	wearable (glove)	pressure	polymer casting	flexible	x	x	x
Truby et al. [6]	soft robotics	pressure, strain	e-3D printing	stretchable	x	o	x
Cheng et al. [18]	robotics (full-body)	multiple	polymer casting	rigid/flexible	x	x	x
Sundaram et al. [19]	wearables (glove)	pressure	sewing	flexible	x	o	x
Wei et al. [7]	wearables (glove)	pressure strain	e-3D printing	stretchable	x	o	x
Park et al. [3]	wearables (fingertip)	pressure	3D printing	stretchable	x	o	x
Karagiorgis et al. [4]	-	pressure	3D printing	flexible	x	o	x
Luo and Wu et al. [9]	robotics, wearables	pressure	machine knitting	stretchable	o	o	x
Ruppel et al. [10]	wearables robotics	pressure	polymer casting	stretchable	o	x	x
Wei et al. [5]	-	pressure	3D printing	flexible	x	√	o
Liu et al. [20]	e-skin	pressure	contact printing	flexible	x	o	x

As part of robotic applications, two key problems in the control of under-actuated robot hands are: 1) the lack of angle sensing at the finger joint level which is crucial for soft grasp control, and 2) missing tactile contact information to enable reflexes and a stable grasp [21]–[24]. To address this, we demonstrate our tactile sensing framework for contact and strain sensors within robotics grasping scenarios. Additionally, with our framework, we show how this could be done in a more automated fashion.

This study provides an end-to-end framework where arbitrary 3D models (e.g., fingers and grasping objects) can be unwrapped (flattened) in order to generate bespoke con-

* Shared first authorship on this paper due to equal contribution.

[1] {sonja.gross, diego.hidalgo-carvajal, silija.breimann, nicolai.stein, amartya.ganguly, djallil.naceri, haddadin}@tum.de, Chair of Robotics and Systems Intelligence, MIRMI - Munich Institute of Robotics and Machine Intelligence, Technical University of Munich (TUM), Munich, Germany.

[2] and also with the Centre for Tactile Internet with Human-in-the-Loop (CeTI).

ductive ink-based contact and strain-sensitive skins manufactured with e-3D printing. Our framework workflow can be seen in Fig. 1 and 2. In this regard, we manufactured strain sensors to measure the change in the PIP (Proximal Interphalangeal) joint angle of an under-actuated robot finger and a human finger as well as silicone-based contact sensors for rigid bodies, where, contact is measured during various grasping scenarios. These examples proffer proof-of-concept, that automatic generation of such skin-like soft sensors can be used for a variety of grasping applications. Our contributions are threefold: (1) we provide the research community with an end-to-end framework to flatten arbitrary 3D objects and generate G-code for customizable sensor patterns, (2) we prove that our semi-automatic e-3D printing method is capable of manufacturing conductive-ink-based, skin like sensors in combination with our framework, (3) we show that such sensors improve the motion accuracy on target joints of under-actuated hands, and enable contact detection on complex surfaces of five objects.

II. Methods

Our framework started with 3D models (.obj files) of solid objects as input and flattened them into 2D surfaces using our object flattening tool[1]. Sensing patterns were added onto these surfaces and converted into G-code manufacturing instructions automatically. This G-code was used by an e-3D printer to deposit the desired sensing patterns into a silicone-filled casting mold shaped like the flattened 2D surfaces. Finally, the resulting skin like sensors enveloped the previously selected objects. The following sections detail each component of this workflow.

A. Object Flattening

The procedure for obtaining 2D representations of 3D object models is termed as UV unwrapping, however, in this paper we refer to it as object flattening as it gives an intuitive meaning for our framework. This phase comprised of two steps, firstly, segmentation, where, the surface of an object was split or cut into smaller sizes, and secondly, parameterization, where, each vertex of a 3D representation was mapped onto a 2D surface. Segmentation was useful for instances in which objects are represented by closed meshes. The object meshes we chose for our study required segmentation as well as parameterization. We segmented our objects manually using Meshmixer. For parameterization was executed with an isometric algorithm that preserves the side lengths of the mesh's triangles, maximizing shape preservation during the flattening procedure. We obtained the best results with Boundary First Flattening (BFF) [11] and Optcuts [14] as described in [25]. We integrated BFF in the flattening tool of our framework using the implementation[2] of [11].

To exhibit the capabilities of our framework, we chose two platonic objects, a cube and a dodecahedron. We included objects with more complex surfaces, namely, a cylinder, a cup and an irregular object (modified version of Jamar hydraulic hand dynamometer, a reference device proposed in the American Society of Hand Therapists [26]). Additionally, we used a 3D scan of a human index finger and the 3D model of a robot hand's index finger (RH8D, Seed Robotics, Portugal). All sensorized objects, the robot and the human finger are displayed in Fig. 2D. The objects were represented by triangular meshes with a resolution ranging from 12 (cube) to 84,982 triangles (Jamar).

Since our focus was shape preservation, we analyzed the resulting isometric distortion [27] of the flattened surfaces as a reference for shape deformation and an indicator for the precision of our flattening [25]. We calculated the singular values σ_1 and σ_2 of the transformation matrix for each triangle and used them to calculate individual distortions using equation (1). For the overall object distortion we summed all distortions weighted by the area of their corresponding triangle as described by [27]. A flawless 3D to 2D flattening would result in a distortion value of 4.

$$\mathbf{d} = (\mathbf{1} + \sigma_\mathbf{1}^{-\mathbf{2}}\sigma_\mathbf{2}^{-\mathbf{2}})(\sigma_\mathbf{1}^\mathbf{2} + \sigma_\mathbf{2}^\mathbf{2}) \quad (1)$$

B. Sensor Patterns and G-Code Synthesis

We extended the flattening tool of our framework with an interactive application, in which users can place customizable sensing patterns (see Fig. 2A-B). After we adjusted the parameters of the patterns and their placement to fit the contact areas on the object's surfaces, the software automatically generated the G-code. The G-code output follows the standard computer numerical control (CNC) programming language with special adaptions to our specific printer. In this study, we manufactured two sensor patterns as depicted in Fig. 2A. The strain pattern consists of four parallel lines to increase its resistance change during stretch. The contact sensor uses a spiral pattern to cover the maximum amount of area, thereby reducing the signal-to-noise ratio. The interface of the flattening tool was built in Python using Tkinter while the 3D rendering relies on Matplotlib. The general sensor parameters are displayed in Fig. 2A; for the robot finger strain sensor we used l_1 = 60 mm, l_2 = 54 mm, and b = 6 mm, while, the human finger strain sensor was smaller with l_1 = 53mm; l_2 = 43 mm and b = 6 mm. The contact sensor parameters for all objects vary from n = 3 mm - 6 mm; x = 1.7 mm - 3.2 mm; b = 1.5 mm - 8 mm; l = 3 mm - 8 mm and s = 10 mm - 45 mm. An overview of the contact pattern size s for each object is stated in Table II; the robot and human finger contact sensors are the smallest with s = 10 mm.

C. Sensor Manufacturing and Data Acquisition

A commercial FDM printer (Ender 5 plus, Creality) was combined with a soft materials print head (vipro-HEAD 3, ViscoTek) to deposit Carbon grease (846-1P, MG Chemicals, resistivity 63 Ωcm) into a two-layer encapsulating silicone matrix as described in [15]. The bottom reservoir layer of higher viscosity (height 2.0 mm) held the conductive ink in place while the top filler layer (height 0.5 mm), filled up the gap created by the nozzle movement. The reservoir layer was prepared by mixing 1 Part A Ecoflex 00 – 30: 1 Part B Ecoflex 00 – 30 + 2 wt% Slo-Jo Platinum Silicone Cure Retarder with 1 wt% Thivex (all reagents from Smooth-On Inc) and degassed it in a vacuum chamber (Vacuum system with pump VP1200 and Thermo Scientific Nalgene vacuum chamber, Silikonfabrik, Germany). The reservoir layer was poured into the relevant casting mould (printed with Polylactide on a Prusa MK3S, Prusa, Czech Republic) and evenly

[1]https://github.com/nicolaistein/TSDF

[2]https://github.com/GeometryCollective/boundary-first-flattening

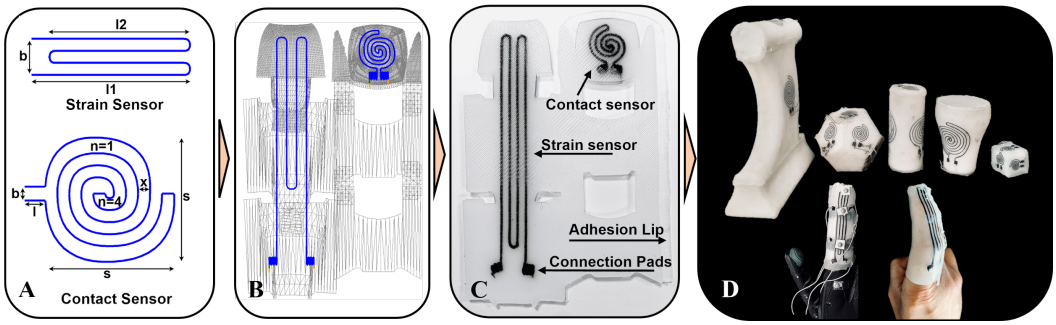

Fig. 2. Overview of sensor designs. A: Parameters of strain and contact sensors B: Pattern placement for the robot finger sensor skin. C: Completed e-3DP printed sensor skin for robot finger. D: Overview of sensorized objects (from left to right: Jammar, dodecahedron, cylinder, cup, cube), sensorized robot and human finger).

distributed using a vortex mixer for (ZX4, VELP Scientifica Srl., Italy). For the filler layer, the mixture consisted of 1 Part A : 1 Part B + 2 wt% Slo-Jo Platinum Silicone Cure Retarder with 10 wt% Silicone Thinner which was also degassed in the vacuum chamber and poured on top of the reservoir. Finally, the printer deposited the carbon grease into the silicone matrix defined by the G-code commands and the sensor was cured for 12h. We set the printing velocity to 100 mm/s for straight lines and 200 mm/s for curved lines with an extrusion factor of 4. The printing height ranged between 1.5 mm and 1.7 mm dependant on manufacturing inaccuracies in the casting molds.

Post curing, 0.25 mm flexible cables were stripped and pierced through the silicone matrix with pliers to connect the underlying carbon grease. Once connected, a drop of FAST Ecoflex 00 - 35 (1 Part A: 1 Part B) was deposited on the interface spot and cured for 2 minutes which sealed the carbon grease and prevented the cables from pulling out of the sensor. The sensor skin was wrapped around the relevant object and glued together with an adhesive lip (see Fig. 2C) using FAST Ecoflex 00 - 35 (1 Part A: 1 Part B) and cured for 2 minutes. All sensors except for the human finger sensor, were glued to the relevant object with silicone adhesive sealant (DOWSIL^{TM} 744, Dow, USA) to prevent movement.

We used custom made Wheatstone bridges to convert sensor electrical resistances into voltage. Bridges were connected to two 16-channel analog multiplexer boards (BOB-09056, Sparkfun. Electronics, USA). A microcontroller board (ATSAME54-XPRO, Microchip Technology Inc., China) read each channel and relayed it via serial communication to a ROS-based interface on a PC with a frequency of 100 Hz.

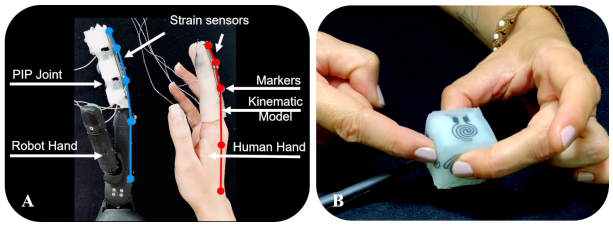

Fig. 3. (A) Experimental setup for human and robot finger strain sensor calibration. (B) Sample experimental setup for contact detection during human manipulation.

D. Experiments

1) Strain Sensor Calibration: We calibrated the strain sensors on both the human and robot fingers with respect to the PIP joint angle of each finger. Fig. 3A depicts the experimental setup. A state-of-the art motion capture system (Vero 2.2; Vicon Motion Systems Ltd, Oxford, UK) with sixteen infrared cameras was used to track the finger movements of the human and robot finger. Our set-up was able to achieve a marker position error < 0.4 mm with respect to the world coordinates. We placed 4 mm radius markers on the human and robot hands in identical locations, similarly to works such as [28]. We performed three trials of flexion-extension motions of the index finger of one subject (female, right handed) and recorded the sensor data and the marker positions from the motion capture system simultaneously. We repeated the same calibration experiment for the RH8D robot hand. The fingers PIP joint angles obtained from the motion capture system served as ground truth during sensor calibration. We calibrated both sensors within the PIP angle range from 10° to 80°. During calibration, the trials were not randomised as the focus was repeatable data that could be used to ensure a suitable characterization curve and subsequently, a robust control. The PIP angle was calculated using the following equation

$$\|\mathbf{V_1} \times \mathbf{V_2}\| = \|\mathbf{V_1}\| * \|\mathbf{V_2}\| * \sin(\alpha) \tag{2}$$

where, $\mathbf{V_1}$ is the vector between the markers from MCP (metacarpophalangeal) to PIP joints, and $\mathbf{V_2}$ the vector from PIP to DIP (distal interphalangeal) joints, respectively. α is the angle between these two vectors. Additional markers were placed on both the human and robot hands. They were recorded to generate the base framework of the finger kinematic model. The kinematic measurements were filtered using a fourth order low-pass Butterworth filter with a cutoff frequency of 5 Hz. Then, the filtered data was used to calculate the fitting curve for the characterization between the relative voltage change $\Delta U/U_0$ measured from the strain sensors and the PIP joint angles.

2) Human-robot finger control scenario: As the robot hand is under actuated, individual control of each finger joint was not possible. We used the strain sensor placed on the human finger to control the corresponding robotic one. We used the characterization curve obtained from the strain sensor on the human finger to calculate the PIP joint angles that the subject executed during flexion-extension trials. The angles were the target PIP joint angles for the robot finger to follow. Target PIP angle values were converted into desired relative voltage change $\Delta U/U_0$ using the inverse characterization curve of the robot finger. A closed loop proportional controller was implemented to match the

desired voltage relative change values. We used ROS to read the sensor signals, and control the robot hand. MATLAB (R2021a, MathWorks, Inc., Natick, Massachusetts, United States) was used for data analysis.

The human-robot finger control experiment had two stages. First, the subject flexed the finger to only move the PIP joint keeping MCP joint fixed. Once the finger was fully flexed, the subject extended it back to its original position. This motion was repeated three times. We fixed the MCP joint of the index finger of the robot to match human motions. We ran the controller and recorded the motions of both the human hand and robot hand fingers with the motion capture system. In the second stage of the experiment, the subject was instructed to move the PIP joint in a random motion, with relatively slow motions at first, followed by faster motions. As before, the controller was left running and kinematic data from both the human and robot finger were recorded.

3) Grasping and Manipulation: In this part we assessed the functionality of our contact sensors. We performed customized human manipulation sequences for each object as depicted in Fig. 3B. During the manipulation sequences, we ensured that the hand touched each sensorized region of the targeted object. Thereby evaluating reliable contact detection of our sensorized silicone skins. We qualitatively marked contact events by recording sensor signal variation and matched them with the corresponding elapsed time. The relative resistance change was normalised with respect to each sensor's recorded maximal relative voltage change to enable equivalent comparison between each surface as well as among each of the five objects.

III. Results

The values of isometric distortion after flattening (using BFF method) for our objects were: cube: 4.0; Jamar: 4.037; cup: 4.039; cylinder: 4.0002; dodechaedron: 4.0; human index finger: 4.042; robot index finger: 4.005.

A. Strain Sensors Calibration

Fig. 4 shows the recorded PIP joint angle of the human finger (A) and robot finger (B) with the corresponding relative voltage change of the sensor $\Delta U/U_0$. The calibration curves consider the angle range from 10° to 80°. Both instances show hysteresis between the flexion and extension phases. The calibration curves characterize the relationship between the PIP joint angles and the relative voltage change at the sensors. As displayed in Fig. 4A, a 3rd-order polynomial fit was performed for the human finger (SSE = 0.04; R^2 = 0.94). The relative voltage of the human finger sensor changes up to $\approx 4\%$ of its initial value with an angular sensitivity that varies from $b_{ang_{min}} = 1.60\times10^{-4}\ deg^{-1}$ to $b_{ang_{max}} = 1.60\times10^{-3} deg^{-1}$ with a mean of $\bar{b}_{ang} = 5.33\times10^{-4} deg^{-1}$. Fig. 4B displays the 4th-order polynomial fit for the robot finger sensor (SSE = 5.40; R^2=0.86). The relative voltage of the robot finger sensor changes up to $\approx 40\%$ which also reflects in the higher angular sensitivity of $b_{ang_{min}} = 8.5°\times10^{-5} deg^{-1}$ to $b_{ang_{max}} = 7.7°\times10^{-3} deg^{-1}$ with a mean of $\bar{b}_{ang} = 4.7\times10^{-3} deg^{-1}$.

B. Human-robot finger position control

Fig. 5 shows that the PIP joint of the robot finger closely follows the corresponding joint on the human finger, particularly during the flexion phase. However, the robot finger saturates above ∼80° as this exceeds the range of the calibration curves and our controller. This, combined with the hysteresis of the strain sensor leads to a delay during extension. The flexion-extension motions were slow with a period of ∼8 seconds for each cycle. Fig. 5B shows the comparison of the PIP joint of the human and robot finger for randomised movements. The figure demonstrates that the robot finger is able to track the human finger PIP joint during slow as well as fast voluntarily controlled movements. The fastest flexion-extension cycle was within ∼1 second. The robot finger was able to follow the human motions accurately with a mean error of 6.61° for uniform motions and 18.77° for randomised motions.

C. Contact Detection

We performed in-hand human manipulation on five objects. Fig. 6 shows the contact detection of three of these objects, namely dodecahedron, cube and Jamar. The manipulation sequence was divided into specific phases with associated images of the trials for clarity. We normalized the sensor scale for the whole sequence between 0 to 1 to effectively compare different sensor signals. In all cases, the signals start at their lowest values at the beginning of the experiment as they were statically placed on a table. All sensors were touched during manipulation. In case of the Jamar and cube, at least a pair of contact sensors were used to hold the object at any given instance to ease manipulation. In case of the dodecahedron, only 8 sensors were added to its faces instead of all 12. Here non-sensorized faces were used to hold the object while touching sensorized faces individually and then in a randomised fashion. All of the object bottom surfaces were sensorized which caused a minimal distortion in the corresponding contact sensors when the object was placed back on the table at the end of each trial. The manipulation experiments were repeated five times per object. To evaluate the stability of contact estimation of each sensor, we calculated the mean resistance and standard deviation at stable contact over five trials and reported them in Table II.

TABLE II

Characteristics of each contact sensor for five objects.

Sensor Channels	Sensor Parameters	Objects				
		Cup	Cylinder	Jammar	Cube	Dodecahedron
S1	s [mm]	15.0	20.0	32.0	15.0	22.0
	R_0 [kΩ]	545.4	28.9	20.2	44.5	23.9
	$(\overline{R}_c \pm \sigma_c)$[kΩ]	1137.2±110.3	31.9±5.1	28.6 ±2.9	72.7±4.6	46.6±1.6
S2	s [mm]	45.0	45.0	38.0	15.0	22.0
	R_0 [kΩ]	2833.2	593.6	269.8	434.4	159.5
	$(\overline{R}_c \pm \sigma_c)$[kΩ]	3330.9±138.0	723.5±48.4	318.6±13.6	365.4±65.6	207.9±29.9
S3	s [mm]	45.0	45.0	38.0	15.0	22.0
	R_0 [kΩ]	1194.1	1249.3	384.0	634.9	228.0
	$(\overline{R}_c \pm \sigma_c)$[kΩ]	1356.5±31.5	1375.9±99.5	454.1±27.4	1202.5±140.0	292.5±14.9
S4	s [mm]		20.0	38.0	15.0	22.0
	R_0 [kΩ]		189.2	342.3	653.2	109.0
	$(\overline{R}_c \pm \sigma_c)$[kΩ]		197.3±4.4	373.7±8.3	927.0±145.1	126.6±2.9
S5	s [mm]				15.0	22.0
	R_0 [kΩ]				503.0	112.9
	$(\overline{R}_c \pm \sigma_c)$[kΩ]				990.9±182.0	132.6±6.4
S6	s [mm]				15.0	22.0
	R_0 [kΩ]				19.2	88.7
	$(\overline{R}_c \pm \sigma_c)$[kΩ]				10.5±2.1	68.1±5.6
S7	s [mm]					22.0
	R_0 [kΩ]					291.4
	$(\overline{R}_c \pm \sigma_c)$[kΩ]					466.5±91.9
S8	s [mm]					22.0
	R_0 [kΩ]					109.6
	$(\overline{R}_c \pm \sigma_c)$[kΩ]					124.6±7.7

IV. Discussion and Conclusion

We proposed a semi-automatic framework to generate skin-like contact and strain sensors for arbitrary solid objects. Our current framework requires manual intervention for the following: segmentation of object shapes, placement of sensor patterns, preparation of the silicone matrices, wiring of the electrical interface and wrapping of the sensors

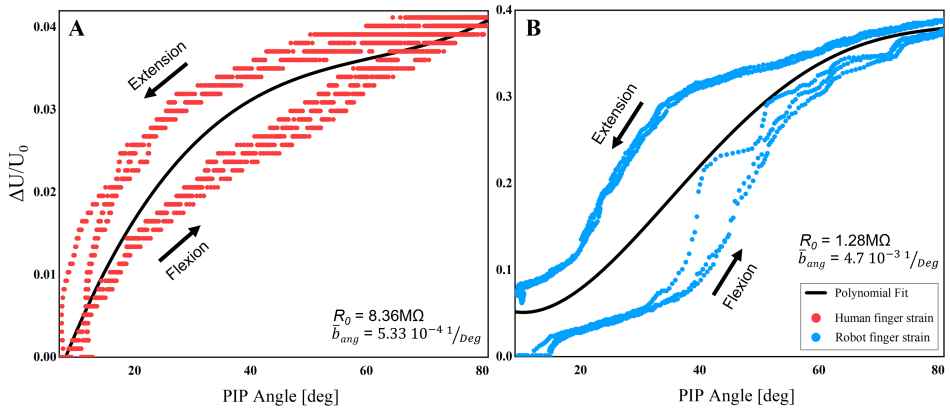

Fig. 4. Calibration of strain sensors. Characterization between PIP joint angle and sensor relative voltage change. A depicts data for the human finger, and B for the robot finger strain sensors. Initial resistances R_0 and mean angular sensitivities $\bar{b}_{ang}$ are also shown.

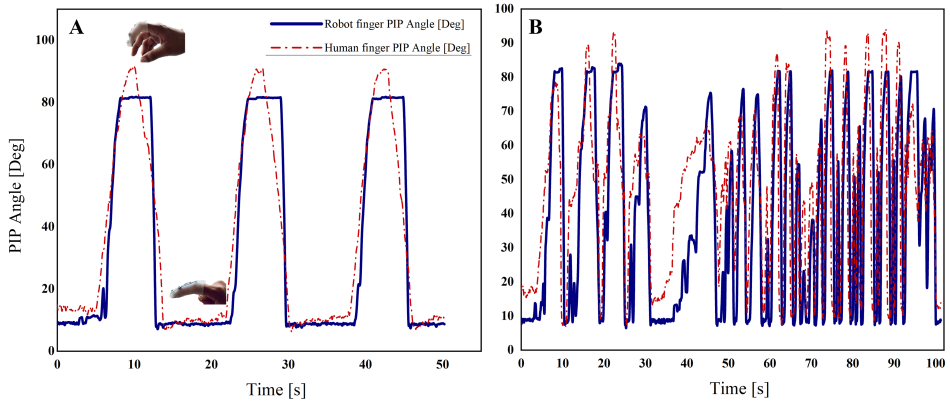

Fig. 5. Human-robot finger control scenario. Comparison of PIP angle between a human finger and its robot hand counterpart during 3 flexion and extension cycles (A) and random slow and fast movements (B). Mean angle error of 6.61° for (A) and 18.77° for (B).

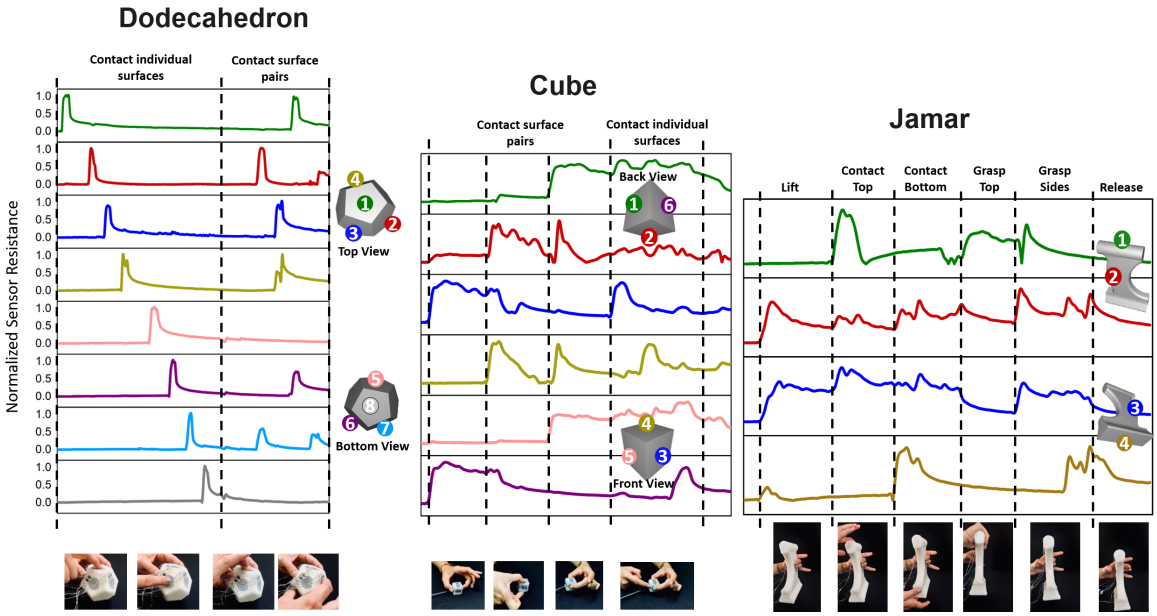

Fig. 6. Contact Detection. Normalized sensor signals during in-hand manipulation scenarios for the Dodecahedron (left), Cube (middle), and Jamar (right).

around objects. Nevertheless, our results serve as proof of concept that our framework has the capability to diversify and expedite the design and fabrication of sensitive skins. Compared to the current state of research, where commonly sensors are manually designed using CAD/CAM [8] and manufactured with multi-step elastomer casting processes [10], our work evolves automatic design and manufacturing methods as proposed by [5].

We demonstrated that objects represented by meshes of diverse resolution, were flattened accurately (distortion values ∼4.0, the ideal isometric distortion value [27]). We used isometric parameterization algorithms that bend the surface of an object and fit it into a 2D surface, whereby closed object shapes require manual segmentation beforehand. An

important observation was that for the flattening of platonic objects, the best results were obtained when BFF was used with the number of cone singularities (which reduce area distortion in presence of high curvature) corresponding to the number of vertices in the objects, i.e. 8 for the cube and 20 for the dodecahedron. The G-code generated with our tool was directly run by the e-3D printer to manufacture the sensors. Although the G-code follows language conventions for computerized numerically controlled machines, some tuning might be required on the G-code generation rules if other 3D printers are used. The fabrication accuracy represented by the standard deviation of the sensors resistance for similar pattern sizes ranged between $\overline{R}_0$ = 332 $k\Omega$±47.2 $k\Omega$ and $\overline{R}_0$ = 1.47 $M\Omega$±0.83 $M\Omega$. Compared to other e-3D printing fabrications for strain sensors as shown in [8] with $\overline{R}_0$ = 60 $k\Omega$±3$k\Omega$, our fabrication is less accurate. A reason for that is the design of our electrical interface. The hard-soft interface between cables and the sensor's connection pads (see Fig. 2C) showed low robustness which led to a decreased connectivity and hence higher initial resistances. Even though adhering the skins to the objects decreased the cable displacements, mechanical pressure on the sensors lead to the same effect. Therefore, we developed an alternative electrical interface: we sewed conductive thread onto the connection pads and mechanically decoupled it with additional stitches. This method led to more robust interfaces. Future research will include e-3D printing of the electrical interface from the sensor pads to prevent fragile hard-soft interfaces and improved manufacturing repeatability to ensure consistent sensor quality and transferable calibration.

State-of-the-art under-actuated robot hands, such as the SoftHand and the Hannes Hand, [22], [23], are not equipped with individual finger joint angle encoders and lack independent joint position control. One contributing factor for the lack of such sensors are narrow space constraints at the joints. Frameworks, such as ours could be used to bridge this gap. Custom strain sensitive sensors that are placed around - not within - the phalanges can be calibrated to reflect the joint angles to be controlled. In the case of robot hands with MCP, PIP and DIP control capabilities, individual joint motions need to be mapped to single sensor deformation signals. In order to demonstrate this application, we engineered skin-like stretch sensors to control the PIP joint angle of a robot hand based on the PIP joint motion of a human index finger. We were able to closely control the PIP joint angle of the robot with a mean angle error deviation of up to 6.61° without the need for encoders. Fig. 5A and 5B show the performance of the index finger PIP joint in the robot hand with respect to its human hand counterpart. We calibrated the stretch sensor curves in the range of 10° - 80° (Fig. 4). The lower limit was chosen to match the lowest observed human finger PIP joint angle during our calibration experiments. The higher limit was chosen to account for the robot finger range of motion, as well as the low sensitivity of the stretch sensors in this region. This explains the robot finger joint saturation when exceeding this range as seen in Fig. 5. The two strain sensors showed different sensitivities; the robot finger sensor was on average ∼8.8 times more sensitive than the human finger one. Two possible reasons were identified: First, the human finger sensor is shorter. This leads to less deformation of the conductive channels during flexion and hence to a lower resistance change. Second, unlike the robot finger sensor, the human finger sensor could not be glued to the phalanges. Therefore, slippage could have occurred during flexion. Future wearable sensor skins should be mechanically fastened to prevent slippage (e.g. whole glove instead of finger cover). The hysteresis of the stretch sensors was a major limitation for the control of the robot finger leading to less accurate results during extension. Although this behavior was stated for other resistive strain sensors in the past [29], this could be overcome by calibrating flexion and extension curves separately and adapting the control accordingly.

In addition to the stretch sensors, we sensorized five objects with soft skin-like contact sensors. During manipulation experiments, we contacted all sensorized regions and evaluated the normalized sensor signals (see Fig. 6). Our sensing skin showed satifactory qualitative contact estimations for all objects. As displayed in table II the mean resistance change at stable contact ranged between 10.1%±7.2% to 108.5%±9.7% of its original value. The least resistance change occurred at the larger sensors with (s=38mm and s=45mm), at which the contacted area is only a small part of the whole sensor, causing low resistance changes compared to the overall resistance. This can be improved by decreasing the size of sensor patterns, thereby increasing the spatial resolution of the contact detection. As evaluated in [15], the current sensor design is not able to measure quantitative pressure due to low sensitivity, sensor drift and relaxation. The characterization of the contact sensors was outside of the scope of this work. Future research will focus on enhancing the sensitivity of the contact detection with alternative sensor materials and morphology to enable quantitative pressure sensing as proposed in [6].

This paper serves as a proof-of-concept in which we successfully demonstrated a multi-disciplinary approach for a semi-automatic method to cover 3D objects with soft skin-like contact and strain sensors. Our framework requires some manual procedures, but significantly reduces the engineering required to develop a bespoke sensor for an arbitrary object. Although, our sensors require advances in sensitivity and more elaborate calibration, they enabled improved control accuracy of an under-actuated robot finger as well as contact detection on arbitrary objects. The proposed method, shows potential for applications in various fields. Especially medical or robotic areas where advanced control or safer user experience is required.

ACKNOWLEDGMENT

We thank Felix Spang and Edmundo Pozo Fortunić for their technical support. This work was funded by the German Research Foundation (DFG, Deutsche Forschungsgemeinschaft) as part of Germany's Excellence Strategy – EXC 2050/1 – Project ID 390696704 – Cluster of Excellence "Centre for Tactile Internet with Human-in-the-Loop" (CeTI) of Technische Universität Dresden. This work was also supported by the Federal Ministry of Education and Research of the Federal Republic of Germany (BMBF) by funding the project AI.D under the Project Number 16ME0539K. We gratefully acknowledge the funding of the Lighthouse Initiative Geriatronics by LongLeif GaPa gGmbH (Project Y).

REFERENCES

[1] P. Roberts, M. Zadan, and C. Majidi, "Soft tactile sensing skins for robotics," *Current Robotics Reports*, vol. 2, pp. 343–354, 2021.

[2] R. Dahiya, N. Yogeswaran, F. Liu, L. Manjakkal, E. Burdet, V. Hayward, and H. Jorntell, "Large-area soft e-skin: The challenges beyond sensor designs," *Proceedings of the IEEE*, vol. 107, pp. 2016–2033, 2019.

[3] S. Park, B. G. Shin, S. Jang, and K. Chung, "Three-dimensional self-healable touch sensing artificial skin device," *ACS Applied Materials and Interfaces*, vol. 12, pp. 3953–3960, 2020.

[4] X. Karagiorgis, M. Ntagios, P. Skabara, and R. Dahiya, "3d-printed elastomer foam-based soft capacitive pressure sensors," in *2022 IEEE International Conference on Flexible and Printable Sensors and Systems (FLEPS)*, 6 2022, pp. 1–4.

[5] D. Wei, R. Zhang, J.-T. Lin, D. Ratnayake, O. O. Olowo, A. S. Nimon, M. Alqatamin, A. Sherehiy, and D. O. Popa, "Automated fabrication of tactile sensors using a custom additive manufacturing platform," in *2022 International Conference on Manipulation, Automation and Robotics at Small Scales (MARSS)*. IEEE, 7 2022, pp. 1–6. [Online]. Available: https://ieeexplore.ieee.org/document/9870485/

[6] R. Truby, "Embedded three-dimensional printing of autonomous and somatosensitive soft robots," Doctoral dissertation, Graduate School of Arts & Sciences, 2018.

[7] P. Wei, X. Yang, Z. Cao, X. L. Guo, H. Jiang, Y. Chen, M. Morikado, X. Qiu, and D. Yu, "Flexible and stretchable electronic skin with high durability and shock resistance via embedded 3d printing technology for human activity monitoring and personal healthcare," *Advanced Materials Technologies*, vol. 4, pp. 1–9, 2019.

[8] J. T. Muth, D. M. Vogt, R. L. Truby, Y. Menguç, D. B. Kolesky, R. J. Wood, and J. A. Lewis, "Embedded 3d printing of strain sensors within highly stretchable elastomers," *Advanced Materials*, vol. 26, pp. 6307–6312, 2014.

[9] Y. Luo, K. Wu, T. Palacios, and W. Matusik, "Knitui: Fabricating interactive and sensing textiles with machine knitting," in *Proceedings of the 2021 CHI Conference on Human Factors in Computing Systems*, 2021, pp. 1–12.

[10] P. Ruppel, N. Hendrich, and J. Zhang, "Elastic tactile sensor skin on double-curved surfaces for robots and wearables," *IEEE Access*, pp. 1–1, 8 2022.

[11] R. Sawhney and K. Crane, "Boundary first flattening," *ACM Trans. Graph.*, vol. 37, no. 1, dec 2017. [Online]. Available: https://doi.org/10.1145/3132705

[12] B. Lévy, S. Petitjean, N. Ray, and J. Maillot, "Least squares conformal maps for automatic texture atlas generation," *ACM Trans. Graph.*, vol. 21, no. 3, p. 362–371, jul 2002. [Online]. Available: https://doi.org/10.1145/566654.566590

[13] L. Liu, L. Zhang, Y. Xu, C. Gotsman, and S. J. Gortler, "A local/global approach to mesh parameterization," in *Proceedings of the Symposium on Geometry Processing*, ser. SGP '08. Goslar, DEU: Eurographics Association, 2008, p. 1495–1504.

[14] M. Li, D. M. Kaufman, V. G. Kim, J. Solomon, and A. Sheffer, "Optcuts: Joint optimization of surface cuts and parameterization," *ACM Trans. Graph.*, vol. 37, no. 6, dec 2018. [Online]. Available: https://doi.org/10.1145/3272127.3275042

[15] S. Groß, S. Breimann, S. Schwarz, A. Ganguly, and S. Haddadin, "Embedded 3d printing: A cost-effective development platform for tactile sensors," in *Haptics: Science, Technology, Applications, 13th International Conference on Human Haptic Sensing and Touch Enabled Computer Applications, EuroHaptics 2022 Hamburg, Germany, May 22–25, 2022, Proceedings*, H. Seifi, A. M. L. Kappers, O. Schneider, K. Drewing, P. Claudio, A. Abbasimoshaei, G. Huisman, and T. A. Kern, Eds. Springer, 2022, pp. 401–403.

[16] R. Kõiva, R. Haschke, and H. Ritter, "Development of an intelligent object for grasp and manipulation research," in *IEEE 15th International Conference on Advanced Robotics: New Boundaries for Robotics, ICAR 2011*, 2011, pp. 204–210.

[17] G. H. Büscher, R. Kõiva, C. Schürmann, R. Haschke, and H. J. Ritter, "Flexible and stretchable fabric-based tactile sensor," *Robotics and Autonomous Systems*, vol. 63, pp. 244–252, 2015, advances in Tactile Sensing and Touch-based Human Robot Interaction. [Online]. Available: https://www.sciencedirect.com/science/article/pii/S0921889014001821

[18] G. Cheng, E. Dean-Leon, F. Bergner, J. R. G. Olvera, Q. Leboutet, and P. Mittendorfer, "A comprehensive realization of robot skin: Sensors, sensing, control, and applications," *Proceedings of the IEEE*, vol. 107, pp. 2034–2051, 10 2019.

[19] S. Sundaram, P. Kellnhofer, Y. Li, J. Y. Zhu, A. Torralba, and W. Matusik, "Learning the signatures of the human grasp using a scalable tactile glove," *Nature*, vol. 569, pp. 698–702, 5 2019.

[20] F. Liu, S. Deswal, A. Christou, M. S. Baghini, R. Chirila, D. Shakthivel, M. Chakraborty, and R. Dahiya, "Printed synaptic transistor–based electronic skin for robots to feel and learn," *Science Robotics*, vol. 7, no. 67, p. eabl7286, 2022. [Online]. Available: https://www.science.org/doi/abs/10.1126/scirobotics.abl7286

[21] C. Piazza, G. Grioli, M. Catalano, and A. Bicchi, "A century of robotic hands," *Annual Review of Control, Robotics, and Autonomous Systems*, vol. 2, pp. 1–32, 2019.

[22] M. Laffranchi, N. Boccardo, S. Traverso, L. Lombardi, M. Canepa, A. Lince, M. Semprini, J. A. Saglia, A. Naceri, R. Sacchetti, and Others, "The hannes hand prosthesis replicates the key biological properties of the human hand," *Science Robotics*, vol. 5, no. 46, pp. 1–15, 2020.

[23] M. G. Catalano, G. Grioli, E. Farnioli, A. Serio, C. Piazza, and A. Bicchi, "Adaptive synergies for the design and control of the Pisa/IIT SoftHand," *The International Journal of Robotics Research*, vol. 33, no. 5, pp. 768–782, 2014.

[24] W. Chen, Z. Xiao, J. Lu, Z. Zhao, and Y. Wang, "Design and Analysis of a Synergy-Inspired Three-Fingered Hand," in *2020 IEEE International Conference on Robotics and Automation (ICRA)*. IEEE, 2020, pp. 8942–8948.

[25] N. Stein, "Surface mapping of objects for the automatic generation of casting molds for artificial tactile skins," Bachelor's Thesis, Technical University of Munich, 3 2022.

[26] E. Fess, "The effects of jamar dynamometer handle position and test protocol on normal grip strength. proceedings american society of hand therapists," *The Journal of Hand Surgery*, vol. 7, pp. 308–309, 06 1982.

[27] J. Smith and S. Schaefer, "Bijective parameterization with free boundaries," *ACM Trans. Graph.*, vol. 34, no. 4, jul 2015. [Online]. Available: https://doi.org/10.1145/2766947

[28] A. Ganguly, G. Rashidi, and K. Mombaur, "Comparison of the performance of the leap motion controllertm with a standard marker-based motion capture system," *Sensors*, vol. 21, no. 5, 2021. [Online]. Available: https://www.mdpi.com/1424-8220/21/5/1750

[29] A. Georgopoulou and F. Clemens, "Piezoresistive elastomer-based composite strain sensors and their applications," *ACS Applied Electronic Materials*, vol. 2, pp. 1826–1842, 2020.